Journal of Materials Chemistry C

ROYAL SOCIETY OF CHEMISTRY

PAPER

View Article Online
View Journal

Cite this: DOI: 10.1039/d0tc04193a

Gate-tunable two-dimensional superconductivity revealed in flexible wafer-scale hybrid structures†

Xiaowen Han,‡[ab] Min Gao,‡[ab] Yufeng Wu,[c] Gang Mu,[a] Miao Zhang,[a] Yongfeng Mei,[d] Paul K. Chu,[e] Xiaoming Xie,[a] Tao Hu*[c] and Zengfeng Di*[a]

Received 3rd September 2020,
Accepted 1st October 2020

DOI: 10.1039/d0tc04193a

rsc.li/materials-c

Superconducting devices such as superconducting quantum interference devices, superconductor nanowire single photon detectors, and superconducting quantum chips have unique performances not available in conventional semiconductor devices. However, most of the superconducting devices are fabricated on rigid substrates consequently limiting applications requiring mechanical flexibility. Herein, wafer-scale flexible superconducting devices are designed and constructed based on a two-dimensional (2D) superconducting system consisting of superconducting discrete Pb nano-islands and single-crystalline graphene on a stretchable parylene C substrate. Owing to the perfect two-dimensional electron gas (2DEG) provided by single-crystalline graphene, the discrete Pb nano-islands are coupled to form a global zero-resistance superconducting state in the hybrid system. Since the discrete island structure is integrated with flexible graphene and parylene C, the superconducting device works steadily even in the bent state. In addition, the Berezinskii–Kosterlitz–Thouless (BKT) type phase transition, the hallmark of two-dimensional superconductivity, can be tuned by the back-gate bias. Our results suggest a convenient and effective strategy to design and prepare large-scale and flexible superconducting systems.

Superconductors can transmit electrical energy with no dissipation and possess unique quantum effects which can be utilized to fabricate superconducting devices such as superconducting quantum interference devices,[1,2] superconducting nanowire single photon detectors,[3,4] superconducting quantum chips,[5] and so on. At present, most superconducting devices are built on rigid substrates consequently impeding potential applications requiring mechanical flexibility. As natural flexible superconductors, superconducting nanowire yarns[6] and organic superconductors[7] have been utilized to build functional superconducting devices, but it is challenging to improve the reliability and productivity on the wafer scale due to the complex fabrication process. Large-scale two-dimensional superconductors (2DSC) with mechanical flexibility can constitute the platform to fabricate a large number of flexible superconducting devices with good uniformity. However, current 2DSCs are often mechanically exfoliated from rigid bulk single crystals and so the dimension of exfoliated 2DSC fragment is typically limited to about 100 μm.[8–11] Recent studies show that 2D superconductivity can be obtained from artificial superconducting islands/graphene hybrids,[12–14] thus suggesting a feasible approach to prepare flexible wafer-scale superconductors if the hybrids can be synthesized on stretchable substrates. Nonetheless, direct experimental demonstration of producing a large number of flexible superconducting devices on wafer-scale 2DSC has not been reported.

In this work, flexible superconducting device arrays are fabricated on the wafer-scale 2D Pb nano-islands/graphene/parylene hybrid. The coupling effect between the discrete Pb nano-islands *via* 2DEG provided by single-crystalline graphene gives rise to global 2D superconductivity as evidenced by the BKT phase transition. Moreover, the BKT temperature can be tuned by the gate voltage. This novel structure consisting of the discrete superconducting islands/graphene/parylene hybrid reveals a viable strategy to design and produce flexible 2D superconducting devices with good uniformity.

Fig. 1 shows the schematic illustration of the fabrication process of the wafer-scale flexible 2DSC device arrays. The single-crystalline monolayer graphene is synthesized on the intrinsic Ge(110) substrate[15,16] by chemical vapor deposition (CVD) (A and B) and the 1 μm thick parylene C layer is

[a] State Key Laboratory of Functional Materials for Informatics, Shanghai Institute of Microsystem and Information Technology, Chinese Academy of Sciences, 865 Changning Road, Shanghai 200050, China. E-mail: zfdi@mail.sim.ac.cn
[b] Center of Materials Science and Optoelectronics Engineering, University of Chinese Academy of Sciences, Beijing 100049, China
[c] Beijing Academy of Quantum Information Sciences, Beijing, 100193, China. E-mail: hutao@baqis.ac.cn
[d] Department of Materials Science, Fudan University, Shanghai 200433, China
[e] Department of Physics, Department of Materials Science & Engineering, and Department of Biomedical Engineering, City University of Hong Kong, Tat Chee Avenue, Kowloon, Hong Kong, China

† Electronic supplementary information (ESI) available. See DOI: 10.1039/d0tc04193a

‡ The authors contributed equally to this work.

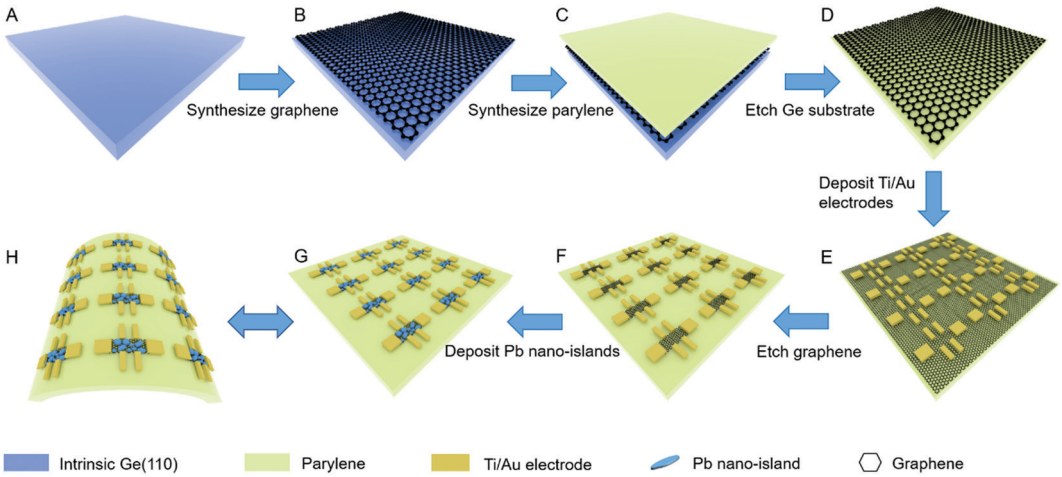

Fig. 1 Schematic illustration of the fabrication process of the wafer-scale flexible 2DSC device arrays: (A) and (B) synthesis of single-crystalline monolayer graphene on intrinsic Ge(110) substrate by CVD; (B) and (C) 1 μm thick insulating parylene C is coated on graphene; (C) and (D) flexible graphene/parylene structure obtained after removal of the intrinsic Ge(110) substrate; (D) and (E) Ti/Au (10 nm/100 nm) Hall bar electrodes deposited on the flexible graphene/parylene substrate; (E) and (F) graphene channel of the Hall bar formed by oxygen plasma etching; (F) and (G) 20 nm thick discrete Pb nano-islands deposited onto the graphene channel; (H) flexible wafer-scale 2D superconducting device arrays are produced.

deposited on graphene (B and C) by vaporization.[17] Parylene C is a green polymer with excellent flexibility, good insulating properties, and chemical stability.[17,18] After removal of the Ge(110) substrate by etching, the flexible graphene/parylene structure is obtained (C and D). With the aid of a Hall bar stencil mask, the 10 nm Ti/100 nm Au electrodes are deposited on the graphene/parylene substrate (D and E). By means of oxygen plasma etching, the graphene channel of the Hall bar is formed (E and F). Finally, a 20 nm thick Pb layer is deposited on the channel region of the Hall bar. Owing to the low melting point of Pb[19,20] and poor wettability of Pb on graphene,[14,21] the deposited Pb layer is dispersed randomly forming discrete nano-islands with an irregular shape (F and G). The hybrid structure composed of discrete Pb nano-islands/graphene/parylene can be easily expanded to cover an entire flexible wafer (H).

The synthesized 100 mm wafer-scale flexible 2DSC device arrays in the rolled and flat states are displayed in Fig. 2a and b, respectively. The 2DSC device arrays are ultra-flexible as demonstrated by that they can be rolled into a pencil shape. Raman scattering reveals that the crystalline quality of graphene is preserved after the transfer process[22–26] even in the rolled state (Fig. S1–S3, ESI†). Fig. 2c shows the zoomed image of the 2DSC device arrays. The transition from the deposited Pb layer to discrete Pb nano-islands is evidenced by the corresponding diffuse reflection, where the Hall bar channel region becomes grey (inset in Fig. 2c). The discrete feature of the Pb nano-islands is further confirmed by plane-view scanning electron microscopy (SEM) and 3D atomic force microscopy (AFM), as shown in Fig. 2d and e, respectively. The Pb nano-islands with a diameter of ~200 nm and thickness of ~20 nm are randomly distributed on graphene (inset in Fig. 2e). Our previous study shows the 2DSC device becomes insulating after removal of graphene between neighboring islands by the oxygen plasma confirming the discrete feature of the nano-islands.[14]

The superconducting properties of the flexible 2DSC device in the flat and bent states are investigated and compared in Fig. 3 (Fig. S4, ESI†). The flexible 2DSC device is diced from the 100 mm wafer prior to characterization on the PPMS-9T (Quantum Design). With respect to the flat 2DSC device, the sheet resistance $R_s(T)$ shows a weak temperature dependence in the normal state above ~50 K (the purple dots region) because

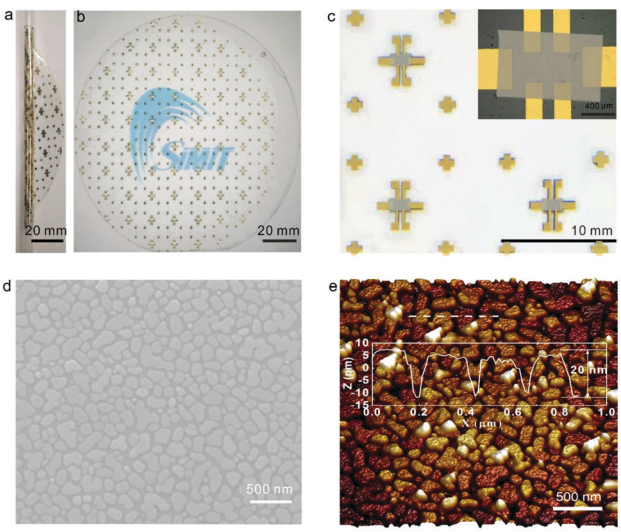

Fig. 2 Demonstration of the wafer-scale flexible 2DSC device arrays: (a) and (b) photograph of the wafer-scale ultra-flexible 2DSC Hall bar device arrays in (a) rolled state and (b) flat state; (c) zoomed image showing the 2DSC Hall bar devices and channel area (inset). In the channel area, the graphene film is invisible and the grey color corresponds to the deposited Pb nano-islands; (d) SEM image and (e) AFM image of the discrete Pb nano-islands deposited on the graphene/parylene film in the channel area. Inset in panel (e): depth profile of the white dashed line in panel (e) showing that the Pb nano-islands have a uniform thickness of ~20 nm and diameter of ~200 nm.

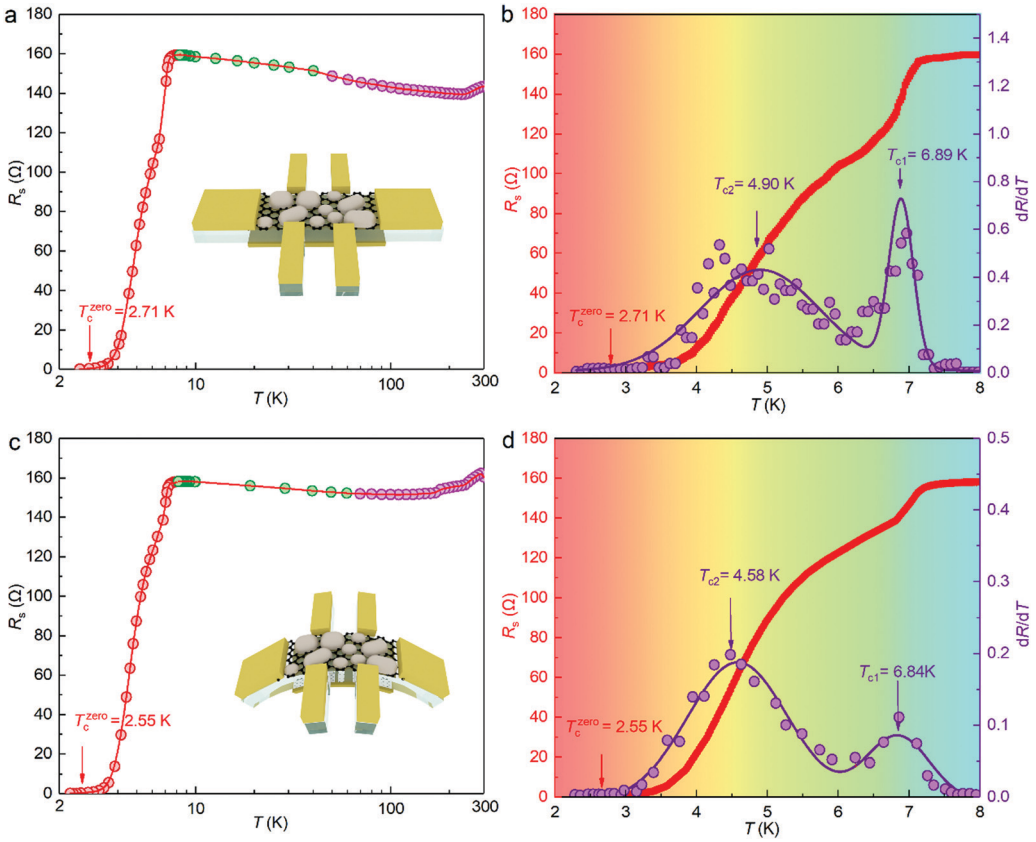

Fig. 3 Superconductivity of the flexible 2DSC device before and after bending: (a), (c) temperature dependent sheet resistance $R_s(T)$ curve of the flexible 2DSC device (a) before bending and (c) after bending measured from 2 K to 300 K. Insets are the schematic diagrams of the devices before and after bending; (b), (d) detailed $R_s(T)$ curve (red line) showing the superconducting region (2 K to 8 K) of the flexible 2DSC device (b) before bending and (d) after bending showing a two-step superconducting transition. The purple dots represent the differential of the $R_s(T)$ curve and the purple lines are the corresponding fitted lines yielding the critical temperatures of the first (T_{c1}) and the second superconducting transition (T_{c2}).

the mobility of graphene is almost temperature independent,[27] as shown in Fig. 3a. As the temperature is reduced, the $R_s(T)$ curve exhibits a semiconductor-like behavior (the green dots region) which can be considered as the weak localization effect of 2D metals.[14,28] Finally, it changes from the superconducting state to the zero-resistance state approaching T_c^{zero} = 2.71 K (the red dots region). In fact, the transition near the zero-resistance state undergoes a two-step superconducting transition[14,21,29] as analyzed in details in Fig. 3b. According to the differential analysis, the first superconducting transition appears at T_{c1} = 6.89 K as a result of the superconducting transition of individual Pb nano-islands.[21] As the temperature is further reduced, the superconducting Pb nano-islands couple with each other to form global superconductivity *via* the 2DEG provided by the single-crystalline graphene. Consequently, the second superconducting transition emerges at T_{c2} = 4.90 K, which corresponds to the onset of the global superconducting phase coherence. Global superconductivity develops as the temperature decreases further and is fully realized at T_c^{zero} = 2.71 K.[12–14,21,29] Furthermore, the superconducting properties of the 2DSC device are retained even in the bent state, as shown in Fig. 3c and d. For the bent 2DSC device, the first superconducting transition emerges at T_{c1} = 6.84 K, which is quite similar to that of the flat counterpart. However, owing to the bending-induced increment of distance between neighboring Pb nano-islands, two critical temperatures (T_{c2} = 4.58 K and T_c^{zero} = 2.55 K) corresponding to onset and completion of the global superconductivity become relatively lower as expected. If the degree of bending state or the curvature can be tuned automatically under cryogenic condition, the distance between the neighboring Pb islands can change continuously, which enables the precise control of two critical temperatures accordingly. It is believed that integration of the flexible components including discrete Pb nano-islands, single-crystalline graphene, and parylene C enables the 2DSC device to operate properly even under bending.

In addition to the flexibility, as an insulating polymer, the coated parylene C can be utilized as a gate dielectric layer.[17] Therefore, the carrier density of the single-crystalline graphene channel can be tuned when a back-gate bias is applied. Fig. 4a shows the $R_s(T)$ curves acquired at different gate voltages between −40 V and 40 V. When the gate voltage is varied, the sheet resistance changes accordingly and the $R_s(T)$ curve exhibits a similar trend with temperature. Since a superconducting islands/graphene system has been reported as a real 2D superconducting system,[12–14] our flexible 2DSC device is

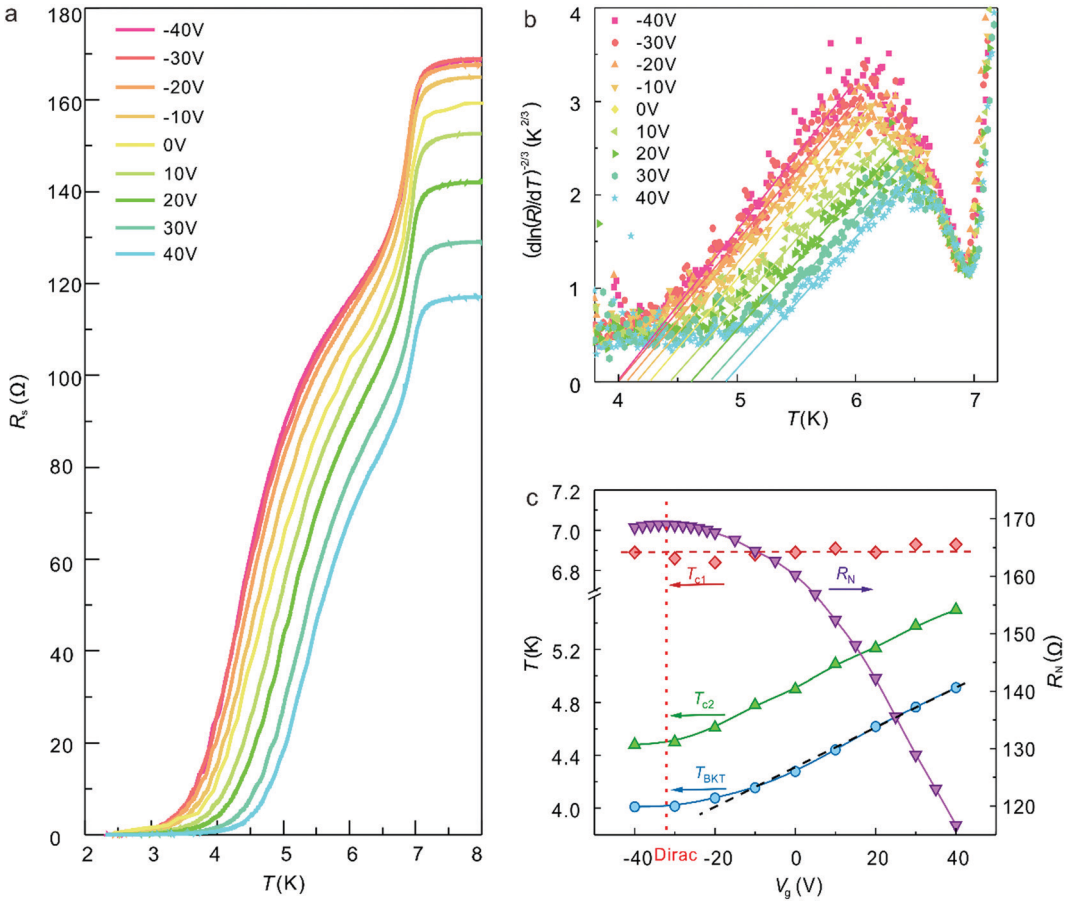

Fig. 4 Gate-tunable 2D superconductivities in the flexible 2DSC device: (a) temperature dependent $R_s(T)$ curves measured under different gate voltages from −40 V to 40 V with the step of 10 V; (b) $R_s(T)$ curves in the form of $[d\ln(R_s)/dT]^{-2/3}$ *versus* T and the vortex-unbinding temperature T_{BKT} is extracted from the x intercept of the linear fit (colored straight lines); (c) T_{c1} (red squares), T_{c2} (green triangles), T_{BKT} (blue dots), and sheet resistance R_N (purple triangles) in the normal state (8 K) as a function of gate voltage with $V_{Dirac} = -32$ V corresponding to the situation in which the Dirac point is located at the Fermi level.

expected to show the Berezinskii–Kosterlitz–Thouless (BKT) type transition.[14,30] The BKT transition describes the free vortex or antivortex at a high temperature forming bounded vortex–antivortex pairs during cooling. The characteristic vortex-unbinding temperature T_{BKT} can be obtained from the V–I measurements[14,31,32] at $V \propto I^3$ or the universal form of the flux flow resistance[21,33] expressed as follows:

$$R_s(T) \propto \exp\left[-b(T - T_{BKT})^{-\frac{1}{2}}\right], \quad (1)$$

where b is a constant. Thus T_{BKT} for each gate voltage can be derived from the x intercept of the linear fits in the plot of $[d\ln(R_s)/dT]^{-2/3}$ *versus* T (Fig. 4b).[12] When cooling down to ~7 K, all the curves converge and show an obvious transition corresponding to the first superconducting transition as discussed above, indicating that the superconducting transition temperature T_{c1} for different gate voltages is similar. As the temperature is reduced further, the converged curves start to disperse. When the temperature enters the region close to the second superconducting transition, the curves are separated due to the change in the carrier density in the graphene channel when a bias is applied. This yields a different BKT temperature for each gate voltage as indicated by the shift in the x intercept.

The derived T_{BKT} is gate voltage dependent and decreases gradually when the gate voltage diminishes from +40 V to −30 V, as shown in Fig. 4c. The dependence of T_{BKT} on the gate voltage becomes less prominent between −30 V and −40 V, where the minimum BKT temperature should exist. Meanwhile, T_{c1} and T_{c2} for each gate voltage are deduced (Fig. S5, ESI†) and plotted in Fig. 4c and T_{c1} is independent of the gate voltages. It can be understood as the first superconducting transition originates from the individual Pb nano-island whose carrier density can be barely tuned by the gate voltage. On the other hand, because the second superconducting transition is related to the coupling effect *via* 2DEG provided by the single-crystalline graphene, the carrier density of the graphene channel and T_{c2} can be tuned effectively by the gate voltage. Thus T_{c2} exhibits a similar variation trend as T_{BKT}, indicating that the BKT transition is also related to the 2DEG in graphene. In addition, manipulation of the carrier density of graphene channel by the gate voltage is evidenced by the variation in

the sheet resistance R_N obtained in the normal state at 8 K (purple triangles), which shows the opposite trend compared to that of T_{BKT}. The maximum R_N at −32 V is reminiscent of the Dirac point of graphene. The relationship between T_{BKT} and the normal sheet resistance R_N can be explained by the universal jump in the superfluid stiffness at the vortex-unbinding transition as shown by the following:[12,34]

$$\frac{T_{c1}}{T_{BKT}}\left\{\frac{\Delta(T_{BKT})}{\Delta(0)}\tanh\left[\frac{\Delta(T_{BKT})}{2k_BT_{BKT}}\right]\right\} = \frac{\varepsilon_v R_N}{R_0}, \quad (2)$$

where $\Delta(T)$ is the superconducting gap and ε_v and R_0 are constants. In this measurement range, T_{c1} of each curve is almost the same and $\Delta(0)$ is also a constant. According to the relationship, if T_{BKT} increases, $\Delta(T_{BKT})$ decreases and $\tanh\left[\frac{\Delta(T_{BKT})}{2k_BT_{BKT}}\right]$ decreases, thus R_N decreases and *vice versa*. Therefore, the T_{BKT} curve is correlated negatively with the normal sheet resistance R_N curve based on the theoretical analysis which is consistent with our experimental results shown in Fig. 4c. The sheet resistance R_N in fact reflects the carrier density n_{2D} in graphene as $R_N \propto \frac{1}{n_{2D}}$ at low temperatures,[35] which is a direct parameter tuned by the gate voltage. Therefore, T_{BKT} shows a positive relationship with n_{2D}. Since n_{2D} of graphene is proportional to $|V - V_{Dirac}|$[27,36] and T_{BKT} is nearly linear with the gate voltage as indicated by the black dashed line in Fig. 4c, $T_{BKT} \propto n_{2D}$ can be obtained. The relationship of $T_{BKT} \propto {n_{2D}}^{2/3}$ has been observed from the MoS_2 transistor[36] and $LaAlO_3/SrTiO_3$ interface[37] and the exponent 2/3 indicates a clean (or weakly disordered) system[37] consistent with the (2 + 1) D-XY model.[38] While in the highly disordered (dirty boson) system in which Cooper pairs are localized in the insulating phase,[37,39] for example, $NdBa_2Cu_3O_{7-\delta}$ thin film[39] and atomically Pb films,[40] the exponent is 1. The superconducting islands/graphene hybrid is an artificial dirty boson system[14] and so in the flexible Pb nano-islands/graphene/parylene hybrid, we observe $T_{BKT} \propto n_{2D}$ as expected. When the gate voltage approaches the Dirac point, T_{BKT} diverges from the linear relationship with n_{2D}. The divergence may arise from the special round Dirac point as has been observed in the other superconducting-islands/graphene system,[12,13] where the deposited superconducting islands and graphene form a p/n junction on the hole side and p/p junction on the electron side consequently destroying the electron/hole asymmetry of pristine graphene.[13]

In conclusion, we describe a general strategy to fabricate wafer-scale flexible 2DSC device arrays by depositing discrete Pb nano-islands on the ultra-soft graphene/parylene film. The 2DSC devices exhibit robust 2D superconductivity and are operational even in the bent state. Owing to the dielectric property of parylene film, the superconductivity of flexible 2DSC device can be tuned by the gate voltage. Integration of discrete superconducting islands and flexible graphene/parylene is demonstrated to be a viable approach to design and fabricate new 2D superconducting devices.

Conflicts of interest

The authors declare no competing financial interest.

Acknowledgements

The authors acknowledge the Key Research Project of Frontier Science, Chinese Academy of Sciences (QYZDB-SSW-JSC021), National Science and Technology Major Project (2016ZX02301003), National Natural Science Foundation of China (Grant No. 51925208, 61851401, 61974157, 61774163, 11574338), Strategic Priority Research Program (B) of the Chinese Academy of Sciences (XDB30030000), and City University of Hong Kong Strategic Research Grant (SRG) (Grant No. 7005105).

References

1 C. P. Yang, S. I. Chu and S. Y. Han, *Phys. Rev. A: At., Mol., Opt. Phys.*, 2003, **67**, 8.
2 S. J. Asztalos, G. Carosi, C. Hagmann, D. Kinion, K. van. Bibber, M. Hotz, L. J. Rosenberg, G. Rybka, J. Hoskins, J. Hwang, P. Sikivie, D. B. Tanner, R. Bradley and J. Clarke, *Phys. Rev. Lett.*, 2010, **104**, 4.
3 T. Yamashita, S. Miki, K. Makise, W. Qiu, H. Terai, M. Fujiwara, M. Sasaki and Z. Wang, *Appl. Phys. Lett.*, 2011, **99**, 3.
4 L. B. Zhang, M. Gu, T. Jia, R. Xu, C. Wan, L. Kang, J. Chen and P. Wu, *IEEE Photonics J.*, 2014, **6**, 8.
5 J. Majer, J. M. Chow, J. M. Gambetta, J. Koch, B. R. Johnson, J. A. Schreier, L. Frunzio, D. I. Schuster, A. A. Houck, A. Wallraff, A. Blais, M. H. Devoret, S. M. Girvin and R. J. Schoelkopf, *Nature*, 2007, **449**, 443.
6 J.-G. Kim, H. Kang, Y. Lee, J. Park, J. Kim, T. K. Truong, E. S. Kim, D. H. Yoon, Y. H. Lee and D. Suh, *Adv. Funct. Mater.*, 2017, **27**, 1701108.
7 J. Wusten and K. Potje-Kamloth, *J. Phys. D: Appl. Phys.*, 2008, **41**, 8.
8 M. Liao, Y. Zhu, J. Zhang, R. Zhong, J. Schneeloch, G. Gu, K. Jiang, D. Zhang, X. Ma and Q. Xue,, *Nano Lett.*, 2018, **18**, 9.
9 Y. Yu, L. Ma, P. Cai, R. Zhong, C. Ye, J. Shen, G. D. Gu, X. H. Chen and Y. Zhang, *Nature*, 2019, **575**, 7.
10 V. Solovyov and P. Farrell, *Supercond. Sci. Technol.*, 2017, **30**, 014006.
11 H. Tomori, N. Hoshi1, D. Inoue and A. Kanda, *J. Phys.: Conf. Ser.*, 2019, **1293**, 012005.
12 B. M. Kessler, C. O. Girit, A. Zettl and V. Bouchiat, *Phys. Rev. Lett.*, 2010, **104**, 4.
13 Z. Han, A. Allain, H. Arjmandi-Tash, K. Tikhonov, M. Feigel'man, B. Sacépé and V. Bouchiat, *Nat. Phys.*, 2014, **10**, 380–386.
14 Y. B. Sun, H. Xiao, M. Zhang, Z. Xue, Y. Mei, X. Xie, T. Hu, Z. Di and X. Wang, *Nat. Commun.*, 2018, **9**, 2159.
15 J. H. Lee, E. K. Lee, W.-J. Joo, Y. Jang, B.-S. Kim, J. Y. Lim, S.-H. Choi, S. J. Ahn, J. R. Ahn, M.-H. Park, C.-W. Yang, B. L. Choi, S.-W. Hwang and D. Whang, *Science*, 2014, **344**, 286–289.

16 J. Y. Dai, D. Wang, M. Zhang, T. Niu, A. Li, M. Ye, S. Qiao, G. Ding, X. Xie, Y. Wang, P. K. Chu, Q. Yuan, Z. Di, X. Wang, F. Ding and B. I. Yakobson, *Nano Lett.*, 2016, **16**, 3160–3165.
17 M. Kim, A. Shah, C. Li, P. Mustonen, J. Susoma, F. Manoocheri, J. Riikonen and H. Lipsanen, *2D Mater.*, 2017, **4**, 035004.
18 P. Ronseaux, R. Othmen, D. Kalita, Z. Han, L. Marty, N. Bendiab, J. Renard and V. Bouchiat, *J. Appl. Phys.*, 2019, **126**, 165301.
19 S. Rolf-Pissarczyk, J. A. Burgess, J. S. Yan and S. Loth, *Phys. Rev. B: Condens. Matter Mater. Phys.*, 2016, **94**, 224504.
20 T. Nishio, T. An, A. Nomura, K. Miyachi, T. Eguchi, H. Sakata, S. Lin, N. Hayashi, N. Nakai, M. Machida and Y. Hasegawa, *Phys. Rev. Lett.*, 2008, **101**, 167001.
21 A. Allain, Z. Han and V. Bouchiat, *Nat. Mater.*, 2012, **11**, 590–594.
22 L. M. Malard, M. A. Pimenta, G. Dresselhaus and M. S. Dresselhaus, *Phys. Rep.*, 2009, **473**, 51–87.
23 C. Ferrari, *Solid State Commun.*, 2007, **143**, 47–57.
24 C. Ferrari, J. C. Meyer, V. Scardaci, C. Casiraghi, M. Lazzeri, F. Mauri, S. Piscanec, D. Jiang, K. S. Novoselov, S. Roth and A. K. Geim, *Phys. Rev. Lett.*, 2006, **97**, 4.
25 M. Huang, M. Biswal, H. J. Park, S. Jin, D. Qu, S. Hong, Z. Zhu, L. Qiu, D. Luo, X. Liu, Z. Yang, Z. Liu, Y. Huang, H. Lim, W. J. Yoo, F. Ding, Y. Wang, Z. Lee and R. S. Ruoff, *ACS Nano*, 2018, **12**, 6117–6127.
26 B.-J. Park, J.-S. Choi, J.-H. Eom, H. Ha, H. Y. Kim, S. Lee, H. Shin and S. G. Yoon, *ACS Nano*, 2018, **12**, 2008–2016.
27 K. Geim and K. S. Novoselov, *Nat. Mater.*, 2007, **6**, 183–191.
28 L. Vandendries, C. Vanhaesendonck, Y. Bruynseraede and G. Deutscher, *Phys. Rev. Lett.*, 1981, **46**, 565–568.
29 S. Eley, S. Gopalakrishnan, P. M. Goldbart and N. Mason, *Nat. Phys.*, 2012, **8**, 59–62.
30 N. Reyren, S. Thiel, A. D. Caviglia, L. F. Kourkoutis, G. Hammerl, C. Richter, C. W. Schneider, T. Kopp, A.-S. Rüetschi, D. Jaccard, M. Gabay, D. A. Muller, J.-M. Triscone and J. Mannhart, *Science*, 2007, **317**, 1196–1199.
31 W. Tsen, B. Hunt, Y. D. Kim, Z. J. Yuan, S. Jia, R. J. Cava, J. Hone, P. Kim, C. R. Dean and A. N. Pasupathy, *Nat. Phys.*, 2016, **12**, 208.
32 Y. Xing, H. Zhang, H. Fu, H. Liu, Y. Sun, J. Peng, F. Wang, X. Lin, X. Ma, Q. Xue, J. Wang and X. C. Xie, *Science*, 2015, **350**, 542–545.
33 P. Minnhagen, *Rev. Mod. Phys.*, 1987, **59**, 1001–1066.
34 M. R. Beasley, J. E. Mooij and T. P. Orlando, *Phys. Rev. Lett.*, 1979, **42**, 1165–1168.
35 H. Castro Neto, F. Guinea, N. M. R. Peres, K. S. Novoselov and A. K. Geim, *Rev. Mod. Phys.*, 2009, **81**, 109.
36 Q. Chen, J. Lu, L. Liang, O. Zheliuk, A. A. E. Yumin and J. Ye, *Adv. Mater.*, 2018, **30**, 1800399.
37 D. Caviglia, S. Gariglio, N. Reyren, D. Jaccard, T. Schneider, M. Gabay, S. Thiel, G. Hammerl, J. Mannhart and J.-M. Triscone, *Nature*, 2008, **456**, 624–627.
38 S. L. Sondhi, S. M. Girvin, J. P. Carini and D. Shahar, *Rev. Mod. Phys.*, 1997, **69**, 315.
39 M. P. A. Fisher and G. Grinstein, *Phys. Rev. Lett.*, 1988, **60**, 208.
40 W. Zhao, Q. Wang, M. Liu, W. Zhang, Y. Wang, M. Chen, Y. Guo, K. He, X. Chen, Y. Wang, J. Wang, X. Xie, Q. Niu, L. Wang, X. Ma, J. K. Jain, M. H. W. Chan and Q. Xue, *Solid State Commun.*, 2013, **165**, 59–63.

